Original Article

Conceptual Studies Of Biobased Fabrication Of Silver Nanoparticle And Its Delivering Pathway Analysis Inside The Breast Cancer HER2 Protein

P. Sathiya[1], Kannappan Geetha[2*]

[1]PG and Research Department of chemistry, Muthurangam Government Arts College (Autonomous), Vellore – 632 002, Tamilnadu, India. E. mail:sathiya1912@gmail.com
[2*]PG and Research Department of chemistry, Muthurangam Government Arts College (Autonomous), Vellore – 632 002, Tamilnadu, India. E. mail:senthilkgeetha@gmail.com.
Affiliated to Thiruvalluvar University, serkkadu, Vellore.

***Corresponding Authors:** Kannappan Geetha

*PG and Research Department of chemistry, Muthurangam Government Arts College (Autonomous), Vellore – 632 002, Tamilnadu, India. E. mail: senthilkgeetha@gmail.com.
DOI:10.47750/pnr.2023.14.S01.183

Abstract

Breast cancer is one of the most common malignancies among women globally, posing a major public health burden. This study primly aimed to theoretically prove the formation of silver nanoparticles by *Dimocarpus longan* fruit phytoconstituents and the targeted delivery of phytoconstituent by silver nanoparticles inside the cavity of the HER2 protein. The algorithm adsorption location and CHARMm-based docking were used to find the interaction between atoms of 9 phytoconstituents and active site amino acids, respectively. The result of the adsorption locator revealed that silver metal atom π and metal acceptor type interaction with four fragments of Rutin compare to other molecules. The caped complex of silver and Rutin complex CHARMm protocol run resulted that the silver atom standing outside the protein and only the Rutin getting inside the cancer protein HER2's binding pocket formed multiple hydrogen bonds and π-alkyl interaction with the energy of -71.0249 Kcal/mol. The overall result concluded that the Rutin fabricates the silver nanoparticle and the capped silver delivers the Rutin inside the cancer protein HER2's binding pocket. Which leads to the apoptosis of breast cancer cells.

Keywords: Adsorption Locator, CHARMm docking, Silver Nanoparticle, Bio-Interaction, Docking.

INTRODUCTION

The second most common breast cancer takes 7% of the global burden and it is one-fifth of various types of cancers among Indian women. Every year, more than 90,000 new cases of breast cancer are recorded, claiming the lives of over 50,000 women. Biologically and molecularly heterogeneous breast cancers are a group of diseases originating from the breast. [1]**.** Different therapies have emerged in the era of the treatment of breast cancer over the past few years. In addition to being a major contributor to the seriousness of diverse tumors. Breast cancer stem cells (BCSC) provide the most difficult hurdle to cancer treatment. To make treatment more effective, resistance to therapies is the greatest hurdle. Patients with breast cancer might get a variety of treatments. The latest techniques include BCSC-based therapeutics, nanoparticles (albumin, metal, lipid, polymer, and micelle-based nanoparticles), and antibody-drug conjugation systems (ADCs). [2]

Recent advances in nanoparticle-mediated drug delivery are a major factor in the pharmaceutical industry's future and have made a tremendous impact on it [3]. As the most promising field of drug delivery with minimal side effects, nanotechnology-based cancer therapy is one of the most promising [4]. Silver nanoparticles (AgNPs), among the various nanoparticles exploited, are now recognized as promising therapeutic molecules, and their use as drug carriers will undoubtedly grow [5]. Because of their unique physiochemical characteristics, AgNPs have a significant role to play in biology and medicine. Furthermore, they are useful for both passive and active targeting of drugs and have recently been shown to be attractive for the delivery of biomolecules (like proteins, DNA, and RNA), including small drug molecules [6]. In order to treat breast cancer cells, silver nanoparticles can be produced bio-based and then used as drug delivery systems [7]. Previously, we reported that silver nanoparticles derived from *Dimocarpus longan* fruit have cytotoxic properties which inhibit breast cancer cells [8]. Also, the phytoconstituent in fruit extracts such as Epicatechin, Ellagic acid, Gallic acid, Procyanidin C1, Corilagin, Flavogallinic acid, Kaempferol, Quercetin and Rutin [9,10,11] possesses inhibition on cancer. This work primly designed to synthesis silver nanoparticles, to identify which phytoconstituents are responsible for the fabrication of silver nanoparticles. Eventually, the docking studies were performed between HER2 and the best silver-phytoconstituent complex to study the inhibition profile of cancer.

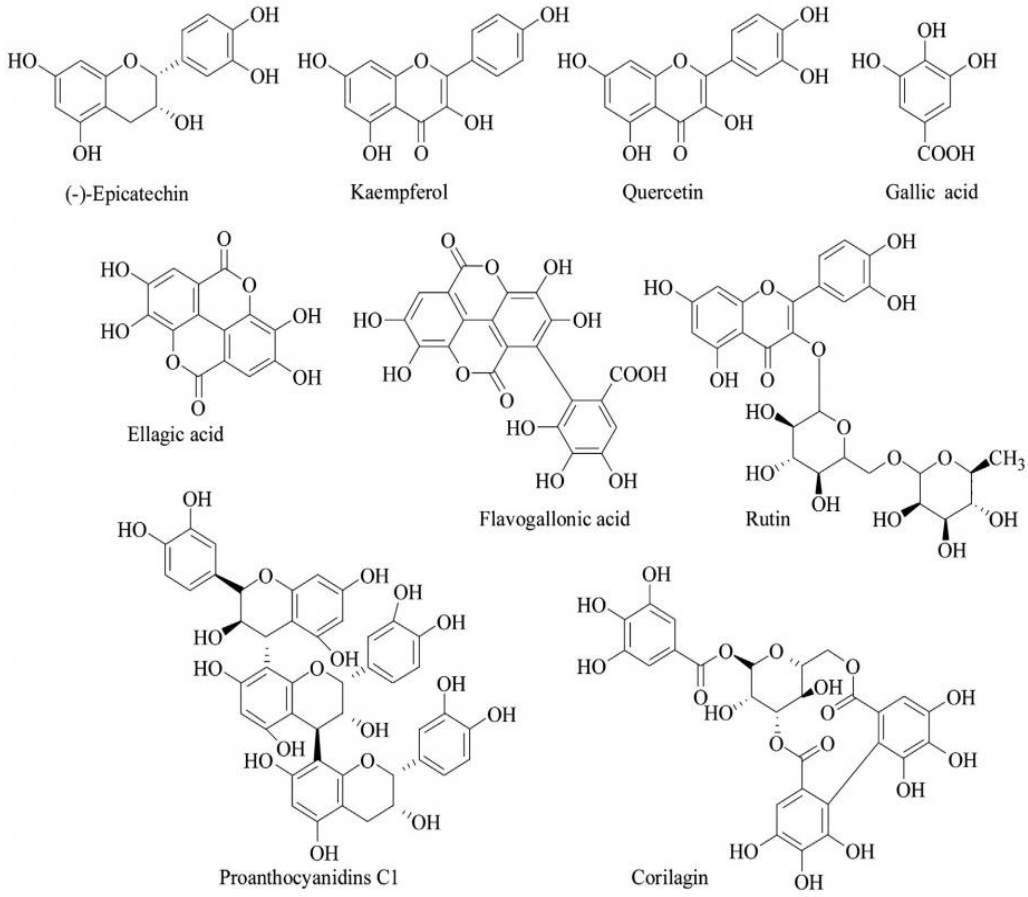

Figure 1 Structure of phytoconstituents of *Dimocarpus longan* fruit

MATERIALS AND METHODS

These studies mainly utilized two major simulation platforms, As first, BIOVIA material studio (v 17.1.0.48) was used for geometric optimization, amorphous cell generation, solvation, silver nanoparticle capping atom identification, and HOMO-LUMO orbital analysis. Secondly, BIOVIA Discovery Studio (v 17.1.0.1643) applied for the interaction evaluation between the Silver-particle, *Dimocarpus longan* components and HER2 protein [12].

Forcite protocol

These traditional molecular mechanics methods primarily calculate energy and optimise geometry for single molecules and periodic systems. In this study, 9 components of *Dimocarpus longan* (Figure 1) and silver nitrate are submitted to forcite calculation. The force field Condensed-phase Optimized Molecular Potentials for Atomistic Simulation Studies (COMPASS) was fixed and the summation of electrostatic and van der Waals by atom-based other parameters was fixed as default (Table 1).

Table 1. Geometric optimization set up for the *Dimocarpus longan* phytoconstituents.

Name of the Parameter	**Setup values**
Force Field	COMPASS
Charges	Force field assigned
Quality	Fine
Summation method	
Electrostatic	Atom-based
Van der Waals	Atom-based

Adsorption location module

A realistic model was created utilising the Amorphous cell platform in MS-2017 to identify the phytoconstituents that are removing silver ions from the solution. The Amorphous Cell component hypothesis first created 3D periodic structures of molecular systems. The cubic cell was filled with silver nitrate ions and all 9 phytoconstituents. The mass density determines the unit cell size, and the number of molecules is automatically chosen. The prescribed mole ratio added water components to the previously vacant surface. The mass density, volume, and mass of the packing zone, which are automatically set, determine the number of molecules.

The location of the silver and nitrate ion with all 9 phytoconstituents in an aqueous environment was examined using the Adsorption Locator procedure after the creation of the amorphous cell. It identifies the low-energy adsorption direction on discrete systems' periodic and nonperiodic substrates. The adsorption locator module operates with three heating cycles, one hundred thousand loading steps, and geometry optimization. In order to measure the overall system energy, simulated annealing was carried out with a modified Monte Carlo step size. Analysis was done on the nonbonded interaction between the nitrate ions and the silver.

DFT calculation

The Calculate Energy (DFT) protocol uses the density functional quantum mechanics method in DMol3 to calculate the energy and optimise the geometry of a group of tiny molecules. Properties such as the total energy, HOMO energy, LUMO energy, dipole, and atomic charges were measured. To start, the 3D structures were loaded individually into Molecule Window. In the simulation, the panel selects the properties which have to be calculated. [13]

Conceptual target inhibition studies

The CDOCKER algorithm is implemented by the Dock Ligands (CDOCKER) protocol. A single protein receptor enables to execution of a refinement docking of any number of ligands. A grid-based molecular docking technique called CDOCKER makes use of CHARMm. The ligands are permitted to flex during the refining while the receptor is kept rigid. The complex of silver and rutin was docked inside the binding pocket of the Minimized HER2 (smart minimizer) protein. High-temperature molecular dynamics produce random conformations from the initial complex ligand structure, which are then followed by random rotations. The random conformations are refined by grid-based (GRID 1) simulated annealing followed by forcefield minimization [14, 15].

RESULTS AND DISCUSSION

Forcite energy and geometric optimization

The forcite protocol run calculated initial structure energy as well as the geometrically optimized final energy of the 9 phytoconstituents. It revealed that the energy of the molecules minimized from the range of -14.8666 – 580.596 kcal/mol to -78.3622 -126.755 kcal/mol were described in (Table 2). These potential energy changes developed due to the electrostatic and van der Waals energy changes including bond angle alteration. [16] (Figure 2). illustrates that the cyclic and aromatic ring system majorly changed their orientation to make the stable molecule of rutin for the further process.

Table 2. Forcite energy of the phytoconstituent of *Dimocarpus longan*.

Name	Initial Potential Energy	Initial RMS Gradient	Electrostatic Energy	Potential Energy	vdW energy	RMS Gradient	Bond Energy
(-)-Epicatechin	52.909	38.498	-18.874	-7.139	1.567	0.008	0.802
Corilagin	580.596	59.696	-171.222	126.775	59.063	0.009	49.017
Ellagic acid	-14.866	44.820	-72.718	-49.721	8.694	0.005	2.825
Flavogallonic acid	266.803	238.879	-117.372	-78.362	12.677	0.009	4.711
Gallic acid	-5.861	39.882	-31.576	-27.241	2.040	0.007	0.314
Kaempferol	65.600	43.599	4.718	18.166	5.079	0.009	1.701
Procyanidin C1	373.441	46.808	-116.582	-43.634	1.343	0.009	6.295
Quercetin	71.982	42.954	-17.777	-6.859	1.697	0.009	1.098
Rutin	225.305	34.569	-46.614	29.241	-2.202	0.009	3.639

*All energies are expressed in Kcal/mol

The Rood mean square deviation RMSD was found to be within the range of 0.00569 to 0.00999. All the bonded and non-bonded energies of a molecule are calculated by the CHARMm energy parameter. Dihedral Energy was found between the range of 73.0402 to 3.64984 kcal/mol. These overall energies conclude that the molecules are well optimized by the smart minimization algorithm.

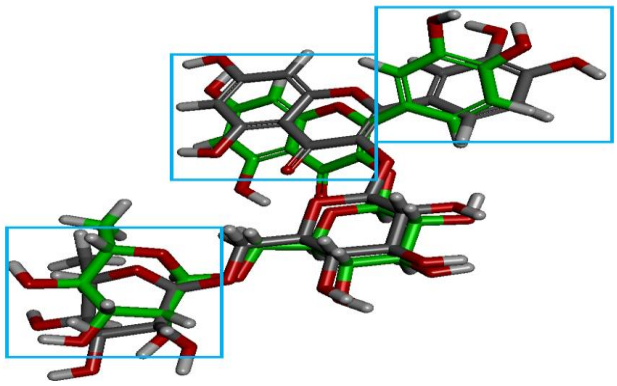

Figure 2. Geometrically Optimized orientation changes of one of the molecules rutin Green (optimized molecule).

Amorphous Cell and Adsorption locator analysis

Amorphous Cells generated the realistic model with 9 phytoconstituents of *Dimocarpus longan* fruit. Further, the boundary box packet with 6534 water molecules and made neutralized with 26 sodium and 17 chloride ions (Figure 3. a - b)

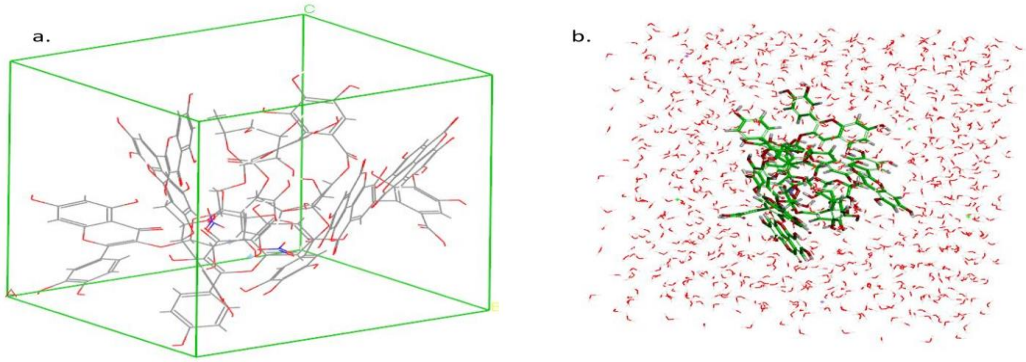

Figure 3. a. Amorphous cell with Phytoconstituents. b. Solvated module with the water molecule

Adsorption locator results revealed the silver ion capping position with each phytoconstituents. Among the 9 phytoconstituent rutin was found better adsorbent of silver compared to others. The silver strongly formed interactions with an aromatic ring position and another oxygen atom of a hydroxyl group (Figure 4. a). The silver ion developed π-interaction with both the benzopyran ring system and -OH group forming an acceptor interaction.

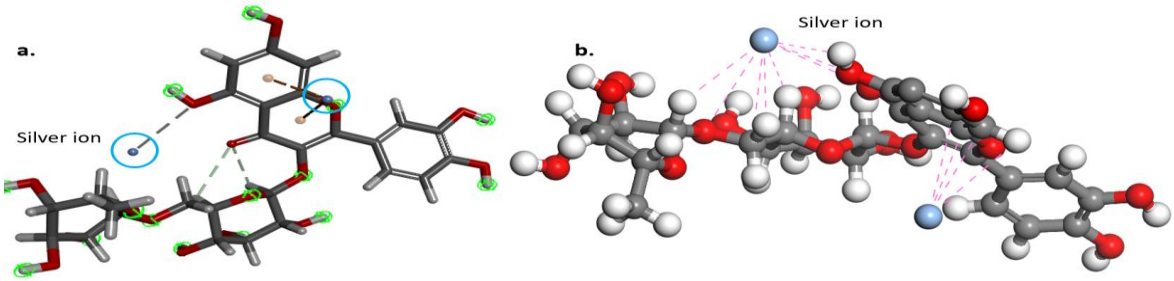

Figure 4. a. silver ion and ring interactions with Rutin molecule. b. Close contacts of the rutin molecule with silver ion.

Table 3. Binding and total complex energy of Phytoconstituents with silver ion.

Name	Total Energy	Binding Energy
Procyclidine	-2066.4138430	-11.1375183
Rutin	-2232.4858676	-14.3700047
Quercetin	-1095.2573189	-6.91335305
Kaempferol	-1020.5563083	-6.73513788
Gallic_Acid	-641.39976036	-3.69759532
(-)-Epicatechin	-1022.8968242	-7.16924717
Flavogallonic	-1695.4731647	-9.74786913
Ellagic_acid	-1129.9173507	-6.41822146
Corilagin	-2076.9824470	-13.6338064

*All energies are expressed in Kcal/mol

Further, multiple close contacts were developed with hydrogen atoms and aromatic ring atoms of rutin molecule in the middle part of the rutin as better absorption compared to the other 8 phytoconstituents of *Dimocarpus longan* fruit (Figure 4. b). The binding and total energy showed that Rutin formed stable energy of -14.3700047 and -2232.489 Kcal/mol after complexation with silver ion. (Table 3)

HOMO/LUMO ORBITAL ANALYSIS USING DFT

By using molecular orbital theory, the reaction mechanism can be explained. The reaction between two molecules occurs when the amount of activation energy overcomes the electronic repulsion by charge attraction or orbital overlap.[17] It is defined as the lowest energy difference between the HOMO (Highest occupied molecular orbital) energy and a molecule's LUMO (Lowest unoccupied molecular orbital) energy. An orbital overlap is necessary for a reaction to occur and the closer the HOMO-LUMO energies of the two molecules, the reaction will occur faster [18]. (Figure 5a. 5b) Illustrates the HOMO and LUMO orbitals of silver nitrate. This analysis illuminates that the LUMO of AgNO3 is primarily composed of an oxygen atom with a contribution of about 87%, [19] whereas HOMO of rutin is mainly composed of H atoms respectively. The bindings occur between the HOMO orbital of rutin and the LUMO orbital of AgNO3. Similarly, other all 9 molecules' orbitals were analyzed and studied the nature orbital.

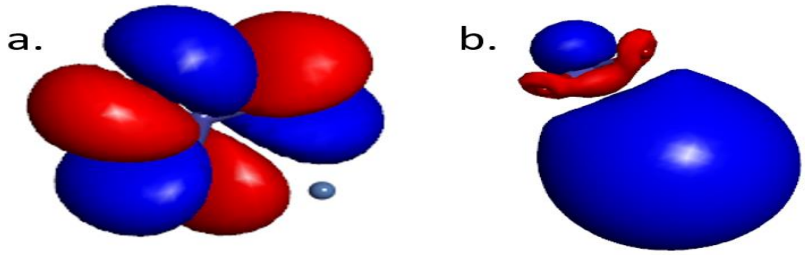

Figure 5. a. HOMO (Red) orbitals of the silver nitrate. B. LUMO (Blue) orbital of the silver nitrate.

The HOMO and LUMO energies of each phytoconstituents remained calculated by means of the DMol3 algorithm. (Table 4) describes the energy difference of each Phytoconstituents of *Dimocarpus longan* fruit. The HOMO and LUMO energy were found to be in the range of -0.18066 Ha to -0.22304 Ha and -0.030369 Ha to -0.11196 Ha. The band gap energy of the molecules indicates the rutin will be the better reactive compared to other phytoconstituents.

The (Figure 6) illustrates the HOMO and LUMO orbitals and it expressed that the rutin molecule possessed orbitals at the edges of the cyclic ring. The remaining fragments of the rutin are free to react with the silver ions LUMO orbitals. The silver ion completely formed a bond with the rutin molecules with the LUMO orbital overlapping. The image proved that the rutin has more affinity and strongly maps with the aromatic ring compared to the nitro ion.

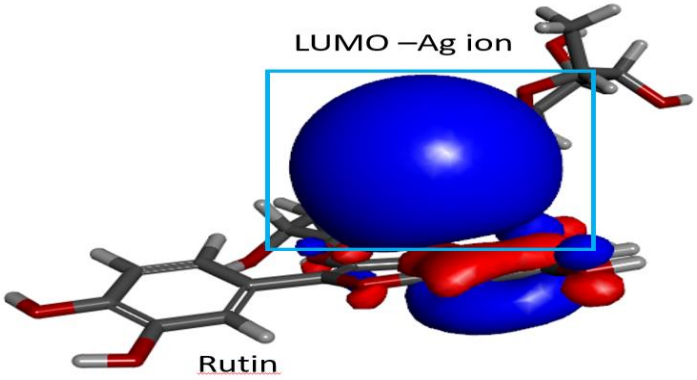

Figure 6. The silver ion caping on the rutin molecule orbital view (HOMO-Red, LUMO -blue).

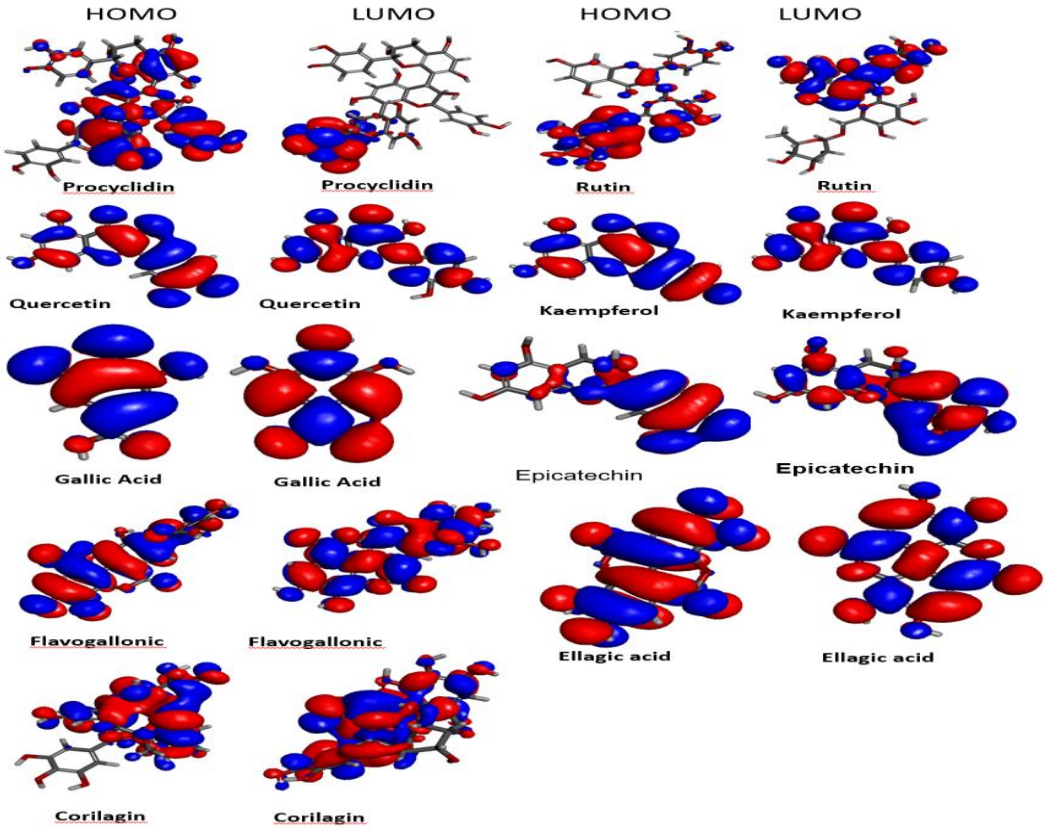

Figure 7. HOMO and LUMO orbitals of all 9 phytoconstituents. (HOMO-Red, LUMO -blue)

Similarly, the procyclidine is filled with HOMO orbitals and free in the LUMO orbital. Other phytoconstituents are mostly composed of both HOMO and LUMO orbitals.

Table 4. DFT energies of 9 Phytoconstituents of *Dimocarpus longan* fruit.

Name	HOMO Energy	LUMO Energy	Dipole Mag	Band Gap Energy
Procyclidine	-0.19302537	-0.04971296	0.52710010	0.10331241
Rutin	-0.22304597	-0.10005867	3.13918738	0.14159730
Quercetin	-0.18128000	-0.08864772	2.05990270	0.09263228
Kaempferol	-0.18407251	-0.08647233	2.39204733	0.09760018
Gallic_Acid	-0.20268183	-0.08027605	0.83207931	0.12240577
(-)-Epicatechin	-0.18845487	-0.03036933	1.75104944	0.15808554
Flavogallonic	-0.21788510	-0.10513257	1.98303162	0.11275253
Ellagic_acid	-0.20304997	-0.11196165	0.00050829	0.11108832
Corilagin	-0.18066331	-0.10127770	2.34404644	0.07938561

*****All energies are expressed in Hartree (Ha)

Interaction analysis inside the cancer protein HER2's binding pocket

The docking protocol run generated the binding of 8 phytoconstituent among the 9 of *Dimocarpus longan* and procyclidine unable to bind due to complex nature and restricted rotation to form proper conformation inside the cancer protein HER2's binding pocket. (Figure 8. a. – b) showed the Secondary structure of minimized HER2 protein with binding pocket and the docked 9 molecules.

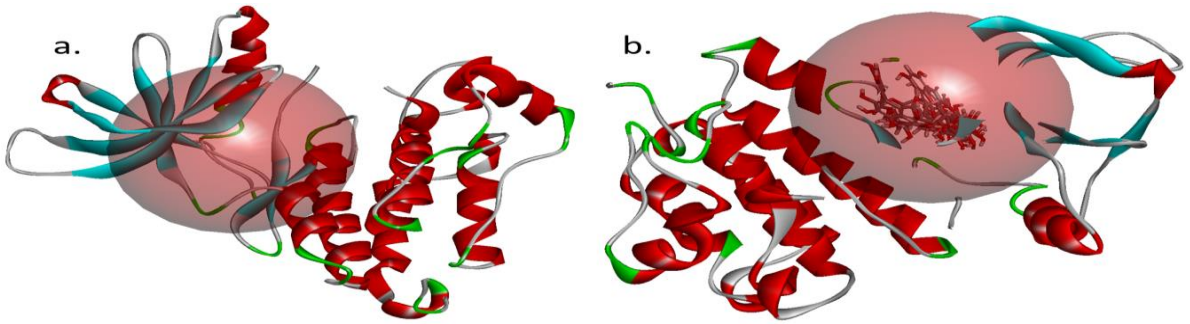

Figure 8 a. Secondary structure of minimized HER2 protein with binding pocket b. Docked 8 molecules inside the cancer protein HER2's binding pocket

The interaction pose analysis showed that Epicatechin formed two types of bonds, Corilagin developed 9 hydrogen bond interactions, which made the molecule bind well but one of the Oxygen atoms in the molecule Acceptor -Acceptor clashed with the Ser783 amino acid reducing the binding. Ellagic acid and gallic acid also formed the same kind of interaction such as hydrogen and π-Alkyl were described in (Table 5). Flavogallonic acid, Kaempferol, and Quercetin have fabricated multiple interactions but unfavorable Acceptor and donor clashes with active site amino acids reduce the affinity (Supplementary Figure 7).

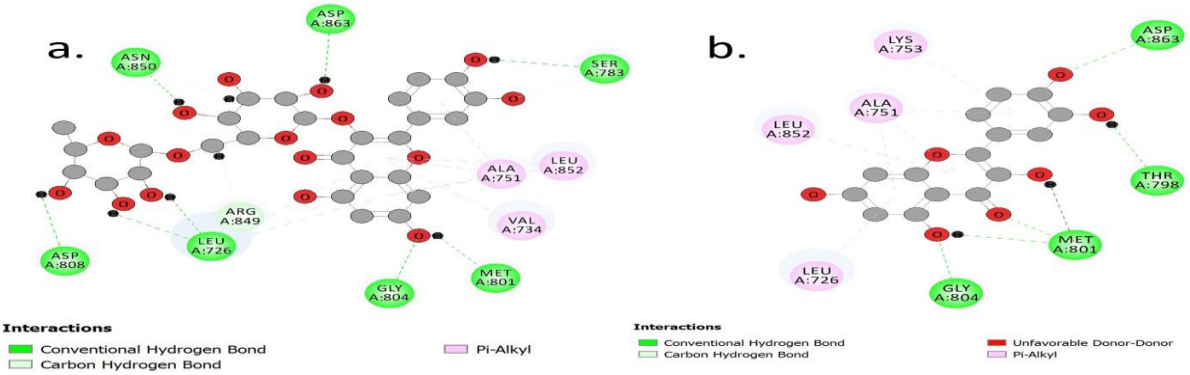

Figure 9. a. Interactions of Rutin with HER2 protein. b. Quercetin interaction with HER2 protein.

The above (Figure 9. a) showed the best binding rutin interactions, which formed 7 conventional hydrogen bonds with Asn850, Asp808, 863, Leu 726, Gly 804, Met 801, and Ser783, 2 carbon-hydrogen bonds, and 6 π-Alkyl interaction with Val734, Ala751, and Leu 852. This binding interaction made the rutin form a proper orientational fit. (Figure 9. b) illustrates quercetin interactions with active site amino acids.

Table 5. Interactions of Phytoconstituents with HER2 protein amino acid.

Phytoconstituent	Type of interactions	Phytoconstituent	Type of interactions
Epicatechin	Hydrogen Bond, π-Alkyl	**Kaempferol**	Hydrogen Bond, π-Alkyl, Unfavorable donor-donor, Unfavorable Acceptor-Acceptor
Corilagin	Hydrogen Bond, π-Alkyl, Unfavorable donor-donor, Unfavorable Acceptor-Acceptor	**Rutin**	Hydrogen Bond, π-Alkyl
Ellagic acid	Hydrogen Bond, π-Alkyl	**Quercetin**	Hydrogen Bond, π-Alkyl, π-Anion, Unfavorable donor-donor
Flavogallonic acid	Hydrogen Bond, π-Alkyl, π-Anion, Unfavorable donor-donor	**Gallic acid**	Hydrogen Bond, π-Alkyl

RUTIN – Ag COMPLEX ANALYSIS

The results of the rutin-Ag complex docking run with HER2 protein exposed that the silver ion delivered the rutin into the binding pocket of the target protein. Also, it aids the protein to change the conformation and forms 6 different kinds of interactions such as hydrogen bonds, conventional hydrogen bonds, and π- type interaction (Figure 10. a - b). Met801, Ala751, and Leu 852 are involved in alkyl interaction with the CH3 fragment of the rutin. Thr862 generates a π-donor hydrogen bond and Cys805 induced π-Sulphur interaction. Ser783, Asp863, Asn850, Thr862, Thr798, and Cys 805 networked with all fragments of rutin and formed stable conformation with the HER2 protein. A comparison of silver complex rutin interaction and normal rutin shows that silver particle delivers the molecule inside the cavity and changes the conformation of HER2. Which leads the molecule to form additional three different kinds of interactions. That silver atom stands outside the protein and only the rutin get inside the binding pocket of the HER2 protein forming multiple hydrogen bond and π-alkyl interaction with the energy of -71.0249 kcal/mol [20].

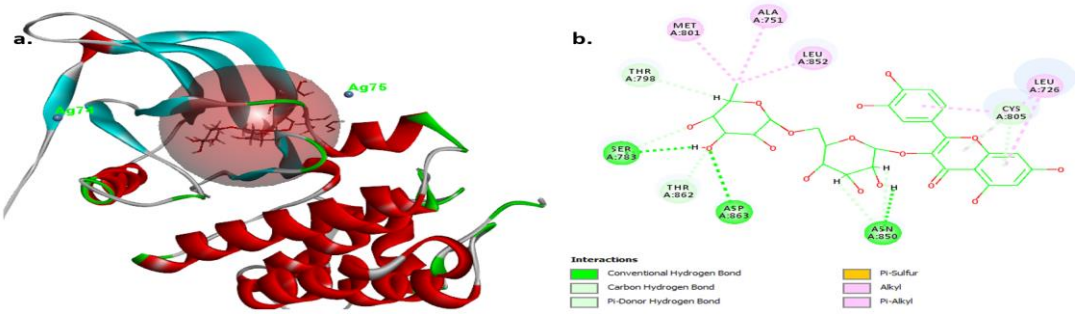

Figure 10. a. Docking of Ag-rutin complex binding with HER2 protein. b. Interactions of rutin with a protein molecule.

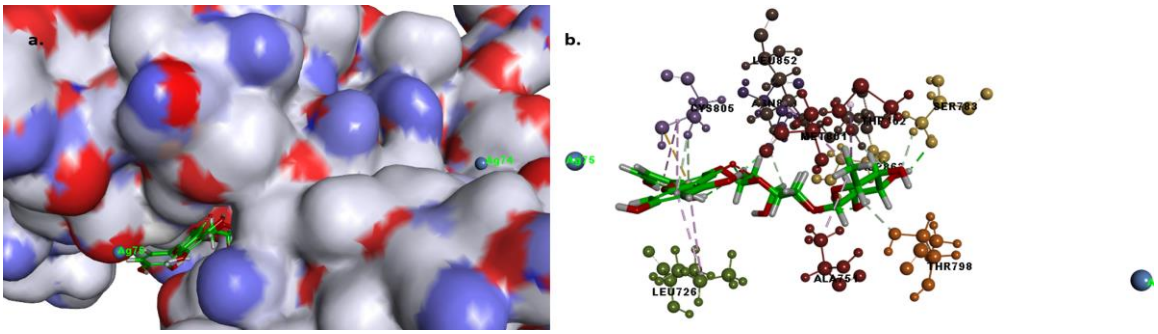

Figure 11. a. Cavity binding of rutin aided by Ag ion. b. Interaction generation by the rutin and the silver ion came outside the binding pocket.

(Figure 11. a-b) demonstrated that Ag aids the rutin molecule to bind inside the hydrophobic cavity of the protein and Two Ag ions came out to the surface of the protein and alter the HER2 protein folding. Which leads to the denaturation and inhibition of breast cancer cell growth.

CONCLUSION

The study concludes that of the 9 molecules tested, rutin capped well with the silver ion leads to the formation of nanoparticles in the adsorption locator protocol run and docking protocol output the silver ion aiding the rutin molecule delivers to bind well inside the cancer protein HER2's binding pocket. This interaction leads to the inhibition of breast cancer cell growth. This theoretical analysis aids the researchers to study and clarify the interaction at the molecular level.

Data and materials availability

All data needed to evaluate the conclusions in the paper are presented in the paper. Additional data related to this paper may be requested from the authors.

Author contributions

All authors have given consent to the final form of the manuscript. P. Sathiya and K. Geetha contributed equally as the first author.

Conflicts of interest

The authors declare that they have no competing interests.

REFERENCE

1. Y. Feng, M. Spezia, S. Huang, C. Yuan, Z. Zeng, L. Zhang, X. Ji, W. Liu, B. Huang, W. Luo, B. Liu, Breast cancer development and progression: Risk factors, cancer stem cells, signaling pathways, genomics, and molecular pathogenesis. Genes & diseases. 5 (2018) 77-106. https://doi.org/10.1016/j.gendis.2018.05.001.
2. K. Barzaman, J. Karami, Z. Zarei, A. Hosseinzadeh, M.H. Kazemi, S. Moradi-Kalbolandi, E. Safari, L. Farahmand, L, Breast cancer: Biology, biomarkers, and treatments. International Immunopharmacology. 84, (2020) 106535. https://doi.org/10.1016/j.intimp.2020.106535
3. J. Conde, G. Doria, P. Baptista, Noble metal nanoparticles applications in cancer. J Drug Deliv. (2012) 751075.https://doi.Org/10. 1155/2012/751075.
4. L. Hasadsri, J. Kreuter, H. Hattori, T. Iwasaki, J.M. George, Functional protein delivery into neurons using polymeric nanoparticles. J Biol Chem. 284 (2009) 6972–6981. https://doi.org/10.1074/jbc.M805956200.
5. M.R. Nasrabadi , S.M. Pourmortazavi , S.A Sadat Shandiz, F. Ahmadi F, H. Batooli H, Green synthesis of silver nanoparticles using Eucalyptus leucoxylon leaves extract and evaluating the antioxidant activities of extract. Nat Pro Res. 28 (2014) 1964–1969. https://doi.org/10.1080/14786419.2014.918124.
6. S. Salehi, SAS. Shandiz, F. Ghanbar, M.R. Darvish, M. Shafiee M. Ardestani, A. Mirzaie, M. Jafari, Phyto-synthesis of silver nanoparticles using Artemisia marschalliana Sprengel aerial parts extract and assessment of their antioxidant, anticancer, and antibacterial properties. Int J Nanomed. 11 (2016) 1835–1846. https://doi.org/10.2147/IJN.S99882.
7. Shafaei, G.R. Khayati, R. Hoshyar, Green and cost-effective synthesis, characterization and DFT studying of silver nanoparticles for improving their biological properties by opium syrup as biomedical drug and good biocompatibility. Inorganic and Nano-Metal Chemistry. (2021) 1-15. https://doi.org/10.1080/24701556.2021.1993257.
8. P. Sathiya, K. Geetha, 2021. Fruit extract mediated synthesis of silver oxide nanoparticles using Dimocarpus longan fruit and their assessment of catalytic, antifungal, antioxidant and cytotoxic potentials. Inorganic and Nano-Metal Chemistry, 52 (2021) 1-11. https: //doi.org/10.1080/24 701556.2021.1983834.
9. X. Zhang, S. Guo, C.T. Ho, N. Bai, Phytochemical constituents and biological activities of longan (Dimocarpus longan Lour.) fruit: A review. Food Science and Human Wellness. 9(2020) 95-102. https://doi.org/10.1016/j.fshw.2020.03.001.
10. P. Paul, P. Biswas, D. Dey, A.S.M. Saikat, M.A. Islam, M. Sohel, R. Hossain, A.A. Mamun, M.A. Rahman, M.N. Hasan, B. Kim, Exhaustive plant profile of "Dimocarpus longan lour" with significant phytomedicinal properties: A literature based-review. Processes. 9 (2021) 1803. https://doi.org/10.3390/pr9101803.
11. J. Wang, D. Guo, D. Han, X. Pan, J. Li, J, A comprehensive insight into the metabolic landscape of fruit pulp, peel and seed in two longan (Dimocarpus longan Lour.) varieties. International Journal of Food Properties. 23 (2020) 1527-1539.https://doi.org/10.1080/109 42912.2020.1815767.
12. N. Irfan, A. Puratchikody, Identification of Silver Nanoparticle-shaping Tridax procumbens Phytoconstituent by Theoretical Simulation and Experimental Correlation. Indian J Pharm Sci. 81 (2019) 900-904. https://doi.org/10.36468/pharmaceutical-sciences.585.
13. Dutta, T., Chowdhury, S.K., Ghosh, N.N., Chattopadhyay, A.P., Das, M. and Mandal, V., 2022. Green synthesis of antimicrobial silver nanoparticles using fruit extract of Glycosmis pentaphylla and its theoretical explanations. Journal of Molecular Structure, 1247, 131361. https://orcid.org/0000-0001-6523-8069.
14. Rudnitskaya, B. Torok, M. Torok, Molecular docking of enzyme inhibitors: A COMPUTATIONAL TOOL FOR STRUCTURE-BASED DRUG DESIGN. Biochemistry and Molecular Biology Education, 38 (2010) 261-265. https://doi.org/10.1002/bmb.20392.
15. A.G.A. El-Helby, H. Sakr, I.H. Eissa, A.S. Al-Karmalawy, K. El-Adl, Benzoxazole/benzothiazole-derived VEGFR-2 inhibitors: design, synthesis, molecular docking, and anticancer evaluations. Archiv Der Pharmazie, 352 (20191) 900178. https://doi.org/10.1002/ardp.201900178.
16. P.K. Panda, P. Kumari, P. Patel, S.K. Samal, S. Mishra, M.M. Tambuwala, A. Dutt, K. Hilscherová, Y.K. Mishra, R.S. Varma, M. Suar, Molecular nano informatics approach assessing the biocompatibility of biogenic silver nanoparticles with channelized intrinsic steatosis and apoptosis. Green Chemistry, 24 (2022) 1190-1210. https://doi.org/10.1039/D1GC04103G.
17. K. Kanagamani P. Muthukrishnan, M. Ilayaraja, K. Shankar, A. Kathiresan. Synthesis, Characterisation and DFT Studies of Stigmasterol Mediated Silver Nanoparticles and Their Anticancer Activity. Journal of Inorganic and Organometallic Polymers and Materials. 28 (2018) 702-10 https://doi.org/10.1007/s10904-017-0721-7.
18. R. Sattari, G.R. Khayati, R. Hoshyar, Biosynthesis and characterization of silver nanoparticles capped by biomolecules by fumaria parviflora extract as green approach and evaluation of their cytotoxicity against human breast cancer MDA-MB-468 cell lines. Materials Chemistry and Physics. 241 (2020) 122438. https://doi.org/10.1016/j.matchemphys.2019.122438.
19. Shafaei, G.R. Khayati, R. Hoshyar, R, Characterization and DFT Studies for Green Synthesis of Silver Nanoparticles by Morphine Ampules and their Anti-proliferation Activity. Journal of Ultrafine Grained and Nanostructured Materials. 53 (2020) 91-97. https://doi.org/10.22059/jufgnsm.2020.01.11
20. T. Dutta, A.P. Chattopadhyay, N.N. Ghosh, S. Khatua, K. Acharya, S. Kundu, D. Mitra, M. Das, Biogenic silver nanoparticle synthesis and stabilization for apoptotic activity; insights from experimental and theoretical studies. Chemical Papers. 74 (2020) 4089-4101.https://doi.org/10.1007/s11696-020-01216-z.